Climate Dynamics
https://doi.org/10.1007/s00382-019-04842-w

Future precipitation changes over Panama projected with the atmospheric global model MRI-AGCM3.2

Shoji Kusunoki[1,2] · Tosiyuki Nakaegawa[1] · Reinhardt Pinzón[3] · Javier E. Sanchez-Galan[4,5] · José R. Fábrega[3]

Received: 13 November 2018 / Accepted: 3 June 2019

Abstract

Future change in precipitation over Panama was investigated with 20-km and 60-km mesh global atmospheric models. The present-day climate simulations were conducted for 21 years from 1983 through 2003, driving models by observed historical sea surface temperatures (SST). The future climate simulations were conducted for 21 years from 2079 through 2099, driving models by future SST distributions projected by the Atmosphere–Ocean General Circulation Models that participated in the Fifth phase of the Coupled Model Intercomparison Project. The uncertainty of future precipitation change was evaluated by ensemble simulations giving four different SST patterns and three different cumulus convection schemes. In the future, precipitation increases over the central and eastern part of Panama from May to November corresponding to the rainy season. Uncertainty of future precipitation change depends on cumulus convection schemes rather than SST distributions. Increase of precipitation over most regions can be attributed to the increase of water vapor transport originated in the Caribbean Sea which converges over Panama. Precipitation averaged over the Panama canal, the Gatun lake and related river basin (79.0°–80.5°W, 8.5°–9.5°N) will increase during most of the rainy season persisting from May to October, while precipitation in dry season persisting from December to April does not change in the future. Intense precipitation increases, but the possibility of drought increases. These results suggest that the planning of water resource management for the Panama canal may require some modifications in the future.

Keywords Precipitation · Panama · Global warming projection · High resolution model

1 Introduction

The climate of the Central America and the Caribbean (CAC) area depends on several large-scale phenomena such as the Inter-Tropical Convergence Zone (ITCZ), North America Monsoon System (NAMS), the El Niño-Southern Oscillation (ENSO) and Tropical Cyclone (TC) activity (Section 14.8.4 in Christensen et al. 2013; Gamble and Curtis 2008; Amador et al. 2016a, b; Maldonado et al. 2018). The air–sea interactions over the warm pool in the tropical eastern north Pacific, the Gulf of Mexico and the Caribbean Sea affect the annual cycle of climate over CAC (Amador et al. 2006; Wang et al. 2007). One of the key element driving climate over CAC is the Caribbean Low Level Jet (CLLJ) which basically originates from easterly trade winds (Amador 1998, 2008) and plays an important role on summer climate over this region (Cook and Vizy 2010). The CLLJ is affected by the coverage and intensity of the Western Hemisphere warm pool (Wang et al. 2008) as well as sea surface temperature (SST) difference across

Electronic supplementary material The online version of this article (https://doi.org/10.1007/s00382-019-04842-w) contains supplementary material, which is available to authorized users.

✉ Shoji Kusunoki
skusunoki@mri-jma.go.jp

1 Global Atmosphere Ocean Research Department, Meteorological Research Institute, 1-1, Nagamine, Tsukuba, Ibaraki 305-0052, Japan

2 Faculty of Societal Safety Sciences, Kansai University, Osaka, Japan

3 Center for Hydraulic and Hydrotechnical Research (CIHH), Technological University of Panama, Panama, Republic of Panama

4 Agroindustrial Research and Production Center (CEPIA), Technological University of Panama, Panama, Republic of Panama

5 Institute of Advanced Scientific Research and High Technology (INDICASAT), Ciudad del Saber, Panama, Republic of Panama

Published online: 12 July 2019

the eastern equatorial Pacific and tropical Atlantic (Taylor et al. 2011; Nakaegawa et al. 2014a). ENSO is a key factor of causing climate variability over the CAC. El Niño brings dry conditions, while La Niña brings wet conditions in the Pacific slope (e.g. Hidalgo et al. 2017).

The country of Panama is situated in the southernmost extent of Central America to the north of the equator (7°–10°N, 77°–83°W). The country is bordered by the Caribbean Sea in the north and by the Pacific Ocean in the south. Since Panama is surrounded by warm tropical oceans, the climate is mainly determined by a hot and humid maritime atmosphere which is typical in most countries of CAC domain (Hastenrath 1978; Ropelewski and Halpert 1987; Nakaegawa et al. 2015). In general, Panama has two precipitation seasons, dry and wet (Taylor and Alfaro 2005). This contrast in precipitation is mainly caused by the northward and southward migration of the ITCZ and is partly affected by other regional phenomena (Magaña et al. 1999; Alfaro 2002; Wang and Enfield 2001; Amador et al. 2006). The dry period persists from December to April in association with the southward migration of the ITCZ from Panama toward the equator. During the wet period from May to November, the ITCZ passes over Panama from the south and moves northward toward the Eastern Tropical Pacific Ocean (Mitchell and Wallace 1992). In Panama including the Panama Canal, the most intense rainfall events in the rainy period often happens in the withdrawal period (Murphy et al. 2014).

The Panama Canal is one of the most important facility in Panama. Income from the passage of vessels contributes about 40% of Gross Domestic Product (GDP) of Panama (https://www.thebusinessyear.com/five-surprising-facts-about-the-panamanian-economy/focus). The primary reservoir for the Canal system is the Gatun Lake which is maintained by inflows from many rivers and streams (Graham et al. 2006). Canal water supply and operations heavily depend on precipitation over the river basin of the Panama Canal (Fábrega et al. 2013). Abundant rainfall amount in Panama is a great advantage for the stable and efficient operation of the Canal. However, precipitation changes due to the global warming may impose restrictions in the future canal operation. Therefore, projection of future precipitation changes is crucial to people and government of the Panama.

Atmosphere–Ocean General Circulation Models (AOGCMs), which were registered in the fifth phase of the Coupled Model Intercomparison Project (CMIP5) and the fifth assessment report of Intergovermental Panel on Climate Change (IPCC AR5; IPCC 2013), simulate reasonably well surface air temperature over the CAC, but the reproducibility of precipitation is low (Table 14.2 in Christensen et al. 2013). The confidence level of simulating TC over CAC is high, but that of simulating ENSO is medium (Table 14.2 in Christensen et al. 2013; Fig. 9.38 in Flato et al. 2013; Hidalgo and Alfaro 2015). Models contributed to CMIP5 simulated well the seasonal March of temperature and precipitation, although they underestimate precipitation from June to October (Fig. 9.38 in Flato et al. 2013). Reasonable simulation of meteorological variables and phenomena affecting climate over the CAC would enhance reliability of future climate change over this region.

Previous generation AOGCMs from the third phase of CMIP (CMIP3) projected a decrease of precipitation over the northern part of the CAC including Panama under the Special Report on Emission Scenario (SRES, IPCC 2000) A1B scenario (Imbach et al. 2012; Hidalgo et al. 2013; Fig. 14.19 in Christensen et al. 2013), which is in line with the negative trend in observation after 1950s (Neelin et al. 2006; Rauscher et al. 2008). The CMIP5 models also projected similar decrease of precipitation over the northern part of the CAC under the Representative Concentration 8.5 (RCP8.5) emission scenario (Fig. 14.19 in Christensen et al. 2013). However, some studies project precipitation increase over the southern part of the CAC including Panama (Hidalgo et al. 2017) and the eastern coast of Costa Rica and Panama (Imbach et al. 2018). High horizontal resolution model of the 60-km mesh Meteorological Research Institute-Atmospheric General Circulation Model (MRI-AGCM3.2H), which is driven by future SST provided by CMIP3 AOGCMs assuming the SRES A1B emission scenario, also project decrease of precipitation over almost all the CAC (Fig. 14.19 in Christensen et al. 2013), The decrease of precipitation over almost all the CAC is consistently projected by CMIP3 24 models, CMIP5 39 models, MRI-AGCM3.1 (Nakaegawa et al. 2014b) and 12 simulations of the MRI-AGCM3.2H (Fig. 14.19 in Christensen et al. 2013). This agreement gives higher reliability of future change in precipitation. Moreover, the higher reproducibility of global precipitation distribution by MRI-AGCM3.2H than by CMIP5 atmospheric models (Kusunoki 2017b) enhance the reliability of the projection.

When we focus on the Panama region, precipitation will consistently increase in future projections by CMIP3 models, CMIP5 models and the MRI-AGCM3.2H, which are totally opposite to the change in the northern CAC regions (Fig. 14.19 in Christensen et al. 2013). Especially, precipitation increase in rainy season from June to September is much larger than in dry season from December to March in terms of hydrological sensitivity defined as precipitation change per 1° warming of surface air temperature (mm day^{-1} C^{-1}). Precipitation increase throughout the year would be favorable for stable and efficient operation of the Panama Canal.

Panama is a relatively small territory with a size of about 600 km in longitudinal direction and the width of about 50–100 km in latitudinal direction. Since the average grid size of CMIP5 models is about 200 km over the CAC, detailed spatial distribution of precipitation change cannot be resolved by these models due to their coarse horizontal resolution. The 20-km and 60-km mesh MRI-AGCM3.2 have great advantage over the CMIP5 models as it can project small-scale distribution of future precipitation change over Panama without the necessity of down scaling using regional climate models. However, previous ensemble simulations by the MRI-AGCM3.2H presented in Fig. 14.19 in Christensen et al. (2013) are forced with CMIP3 SST under the SRES A1B scenario which correspond to previous generation models and scenarios.

The aim of this paper is to project and analyze future precipitation change over Panama, using one of the highest horizontal resolution climate model known as MRI-AGCM3.2 which can resolve small scale structure of orography and precipitation distribution over Panama. Moreover, we aim to update SST boundary conditions projected by the CMIP5 models under the RCP8.5 scenario instead of CMIP3 models under the SRES A1B scenario assumed in previous studies. For the purpose of estimating the uncertainty of future projections, the contribution of future change from the differences in SST distributions and cumulus convection schemes are quantitatively separated.

2 Models and experiments

2.1 The 20-km model

The Meteorological Research Institute—Atmospheric General Circulation Model, version 3.2 (MRI-AGCM3.2S) which has a grid size of 20 km is utilized for experiments. In this paper, we name this model "the 20-km model". It has 60 levels with the highest level of 0.01 hPa corresponding to a height of approximately 80 km. We implemented the cumulus convection scheme called the "Yoshimura scheme" (YS; Yoshimura et al. 2015) which is based on the method proposed by Tiedtke (1989). Using the 20-km model, we have executed a set of global warming projections to investigate future precipitation changes in the CAC (Nakaegawa et al. 2014a; Pinzón et al. 2017), in the Asian region (Endo et al. 2012; Kusunoki and Mizuta 2013; Kusunoki 2016, 2017a; Okada et al. 2017) and over the globe (Kusunoki 2017b).

2.2 The 60-km model

Future climate projection inevitably has uncertainty which is normally estimated by ensemble simulations. Since the 20-km model needs huge computer resources, we could not execute a large number of simulations using the 20-km model. Therefore, we utilized the 60-km mesh size version (MRI-AGCM3.2H) instead of the 20-km model. The 60-km model calculates the time evolution of atmosphere 30 times faster than the 20-km model. The uncertainty of future precipitation changes were evaluated by the ensemble simulation using the 60-km model in previous studies over Asian regions (Endo et al. 2012; Kusunoki and Mizuta 2013; Kusunoki 2016, 2017a) and over the globe (Kusunoki 2017b). As precipitation simulated by models are much influenced by the treatment of cumulus convection process, we also adopted the Arakawa-Schubert (AS) scheme (Randall and Pan 1993) and the Kain-Fritsch (KF) scheme (Kain and Fritsch 1990) scheme to the 60-km model.

The 20-km and 60-km models captures small scale structure of topography and coastal lines of Panama much better than coarser horizontal resolution models (Figs. S1 and S2).

2.3 Sea surface temperature and sea ice

Since our models have no oceans, we have to specify the lower boundary conditions such as sea surface temperature and sea ice concentration. This method is called a 'time-slice experiment' (Bengtsson et al. 2009). In the present-day climate simulation for 21 years from 1983 through 2003, we forced the models with observed historical SST and observed sea ice concentration provided by HadISST1 (Rayner et al. 2003). In the climate modelling community, this kind of experiment is usually called an Atmospheric Model Intercomparison Project (AMIP)-type simulation. This approach is an standard way to evaluate the performance of atmospheric climate models.

In the future climate simulations for 21 years from 2079 through 2099, the lower boundary data of SST consists of three components. First one is the future change taken from CMIP5 28-models' multi-model ensemble (MME) of SST. The second one is the linear trend in the MME of SST projected by the CMIP5 multi-model dataset. The third one is the time series of detrended interannual observed SST anomalies calculated with respect to each month of the period from 1979 to 2003. The difference between the historical experiments and the future simulation by the MME of SST is regarded as the future change in SST. In the future simulations, we assumed the RCP8.5 emission scenario (Collins et al. 2013). Finally, we superposed these three components. Future change in sea ice concentration was constructed by the same method as SST. Mizuta et al. (2008) describes further detail.

Considering the response of models is largely influenced by given SST, the sensitivity of future precipitation change to the geographical distribution of SST is investigated. Clustering analysis is applied to 28 CMIP5 models to separate them into three groups focusing on the future change of annual average SST projected using CMIP5 models in the tropics (Fig. 1a–d). Figure 1e illustrates the difference of SST cluster 1 relative to the mean of all models (C0; Fig. 1a). In the cluster 1 (C1; Fig. 1e), warming in the Southern Hemisphere is larger than in the Northern Hemisphere.

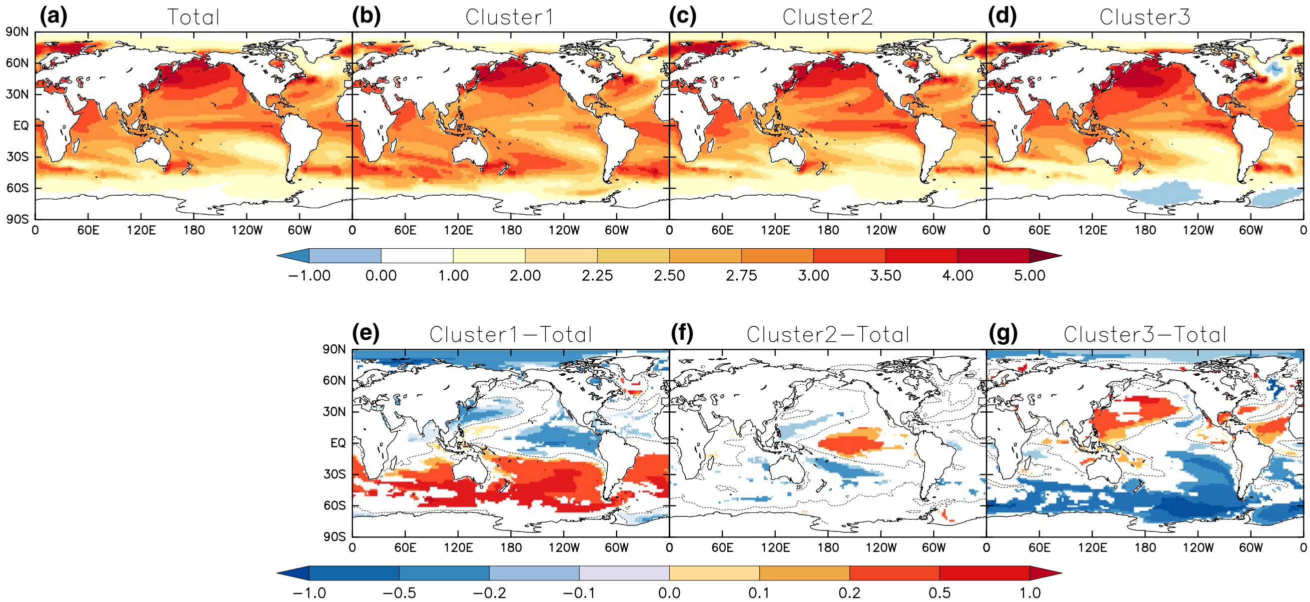

Fig. 1 Distributions of annual mean sea surface temperature (SST) change (K) from the present-day (1979–2003, historical simulation) and the future (2075–2099, RCP 8.5 scenario). **a** The composite of total 28 models (C0). **b** The composite of the cluster C1. **c** C2. **d** C3. **e**–**g** Differences for each cluster from the total mean (C0). The regions where over 75% of the models agree with the sign of the difference are colored. Contours denote zero value. The change is normalized by the tropical (30°S–30°N) mean for each model before making composition, and then multiplied by 28 models mean tropical SST change (2.74 K). From Mizuta et al. (2014)

The cluster 2 (C2; Fig. 1f) is characterized by distinct warming in the central Pacific of the tropics. The cluster 3 (C3; Fig. 1g) is distinguished by conspicuous warming near Japan. The sea ice concentration in the future was created similar to the clustering of SST. Mizuta et al. (2014) describes further details.

2.4 Other external forcings

We have to specify the concentration of greenhouse gases (GHG) which include carbon dioxide and methane. In the present-day climate simulations, observed historical concentrations of these GHG gases were given. In the future climate simulations, the RCP8.5 emission scenario were specified. For natural and anthropogenic aerosol, we utilized 3-dimensional distributions simulated using the MRI-Earth System Model (MRI-ESM; Yukimoto et al. 2011) assuming past historical aerosol emission and the SRES A1B scenario (IPCC 2000). With respect to volcanic aerosols, only the Mt. Pinatubo eruption of year 1991 is included. As for stratospheric ozone, we used the 3-dimensional distributions simulated with the MRI-Chemical Transport Model (CTM) (MRI-CTM; Shibata et al. 2004) assuming past historical aerosol emission and the A1B scenario.

For the consistency of emission scenario used in the whole experimental setting, we should assume RCP8.5 emission scenario to simulate 3-dimensional distributions of aerosol by MRI-ESM and ozone by MRI-CTM. However, we could not afford to execute these simulations due to the limitation of computer resources and time to meet the deadline of CMIP5 mandatory experiments.

2.5 Ensemble simulations

For the purpose of evaluating the sensitivity of model response to the future SST pattern, we have conducted the ensemble simulations forcing the 20-km and 60-km models with four different SST distributions (Fig. 1). In case of the 60-km model, the dependence of model response upon cumulus convection processes was evaluated with the multiple simulations giving three different convection schemes in the present-day climate and the future climate simulations.

In order to estimate and evaluate the uncertainty of simulations due to the internal natural variability of atmosphere, we expanded the present-day climate simulations initiating from different atmospheric initial conditions using the 20-km and 60-km models. Owing to the limitation of computer resources, we could conduct only a single simulation for the future climate. The experimental design and the definition of simulation names are summarized in Table 1. The model and experimental design is the exactly the same as those in Kusunoki (2017a).

Table 1 Definition of simulation names

Model	Grid size (km)	Cumulus convection[a]	Sea surface temperature (SST): Observation by the HadISST1(Rayner et al. 2003)				Ensemble size
Present-day climate: 1983–2003, 21 years							
MRI-AGCM3.2S	20	YS	SPYSnn[b]				2
MRI-AGCM3.2H	60	YS	HPYSnn				2
MRI-AGCM3.2H	60	AS	HPASnn				2
MRI-AGCM3.2H	60	KF	HPKFnn				2
Model	Grid size (km)	Cumulus convection[a]	Sea surface temperature (SST): Projections by the CMIP5 AOGCMs for the emission scenario RCP8.5				Ensemble size
			Cluster 0 MME	Cluster 1	Cluster 2	Cluster 3	
Future climate: 2079–2099, 21 years							
MRI-AGCM3.2S	20	YS	SFYSC0	SFYSC1	SFYSC2	SFYSC3	1
MRI-AGCM3.2H	60	YS	HFYSC0	HFYSC1	HFYSC2	HFYSC3	1
MRI-AGCM3.2H	60	AS	HFASC0	HFASC1	HFASC2	HFASC3	1
MRI-AGCM3.2H	60	KF	HFKFC0	HFKFC1	HFKFC2	HFKFC3	1

First character of simulation name denotes horizontal resolution: S = 20 km, H = 60 km

Second character denotes the target period: *P* present-day, *F* future

Third and fourth characters denote the type of cumulus convection scheme

CMIP5 The fifith phase of the Couple Model Intercomparison Project, *AOGCM* atmosphere–ocean general circulation model, *RCP* representative concentration pathway, *MME*: multi-model ensemble

[a]Yoshiumura (YS): Yoshimura et al. (2015), Arakawa-Schubert (AS): Randall and Pan (1993), Kain-Fritsch (KF): Kain and Fritsch (1990)

[b]nn denotes the number of ensemble member with different atmosphertic initial conditions: nn = 01, 02

3 Observation data to evaluate model performance

We used the One-Degree Daily data (1dd) provided by the Global Precipitation Climatology Project (GPCP) v1.2 made by Huffman et al. (2001) covering 17 years from 1997 to 2013 to evaluate model performance in the present-day climate simulations. Horizontal grid size of this dataset is 1.0° in longitude and latitude, which is equivalent to a interval of about 110 km over the Panama region. As the horizontal resolution of the 20-km and 60-km models is relatively higher than conventional atmospheric models, we choose the GPCP 1ddv1.2 precipitation due to its higher horizontal resolution than other conventional observed precipitation. On the other hand, the GPCP 1ddv1.2 data only cover the part of target period of simulations from 1983 through 2003. Pentad and monthly data are constructed by daily precipitation data. Before the calculation of skill scores, we interpolated model data onto the 1° grid system in the GPCP 1dd data.

The skill of model performance is affected by the selection of observational data, because observations have some ambiguities (Sperber et al. 2013). The monthly data of GPCP v2.2 compiled by Adler et al. (2003) are utilized for 21 years from 1983 through 2003. These data cover the whole period of the present-day simulation (1983–2003). The grid size of this dataset is 2.5°, corresponding to a spacing of about 270 km in the Panama region (Table 2).

The pentad mean and monthly mean dataset of the Climate prediction center Merged Analysis of Precipitation (CMAP) v1201 constructed by Xie and Arkin (1997) are

Table 2 Observational data of precipitation used in this study

Name	Time resolution	Spatial resolution	Period	Region	References
GPCP 1ddv1.2	Day	1.0°	1997–2013, 17 years	Global	Huffman et al. (2001)
GPCP v2.2	Month	2.5°	1983–2003, 21 years	Global	Adler et al. (2003)
CMAP v1201	Month	2.5°	1983–2003, 21 years	Global	Xie and Arkin (1997)
TRMM 3B43 v7	Month	0.25°	1998–2013, 16 years	50°S–50°N	Huffman et al. (2007)

GPCP Global Precipitation Climatology Project, *1dd* the one-degree daily data, *CMAP* climate prediction center merged analysis of precipitation, *TRMM* the tropical rainfall measuring mission also used for 21 years from 1983 to 2003. The grid size of this dataset is 2.5°.

Moreover, monthly mean dataset of the Tropical Rainfall Measuring Mission (TRMM) 3B43 v7 provided by Huffman et al. (2007) are utilized for 16 years from 1998 to 2013. The grid size of this dataset is 0.25° corresponding to a spacing of about 27 km in Panama domain. However, data coverage area is limited to a latitude zone ranging between 50°S and 50°N.

Table 3 compares the characteristics of observational precipitation data referred in the verification of models.

4 Present-day climate

The rainy season of Panama has long duration time from May to November (Enfield and Alfaro 1999; Giannini et al. 2000; Nakaegawa et al. 2015). Figure 2 compares observed precipitation with simulations for summer (June–August) which is in the middle of rainy season over Panama. In the observations by Fig. 2(1)–(3), precipitation is larger on the Pacific Ocean side than on the Caribbean Sea side. In the higher horizontal resolution observation of TRMM by Fig. 2(4), precipitation tends to be smaller over land than

Table 3 Indices of extreme precipitation events

Index	Name	Definition	Unit
PAVE	Annual precipitation	Annual average precipitation	mm day^{-1}
R5d	Maximum 5-day precipitation total	Annual maximum of consecutive 5-day precipitation	mm
PMAX	Maximum 1-day precipitation total	Annual maximum of daily precipitation	mm
CDD	Consecutive dry days	Annual maximum number of consecutive dry days (precipitation < 1 mm)	day

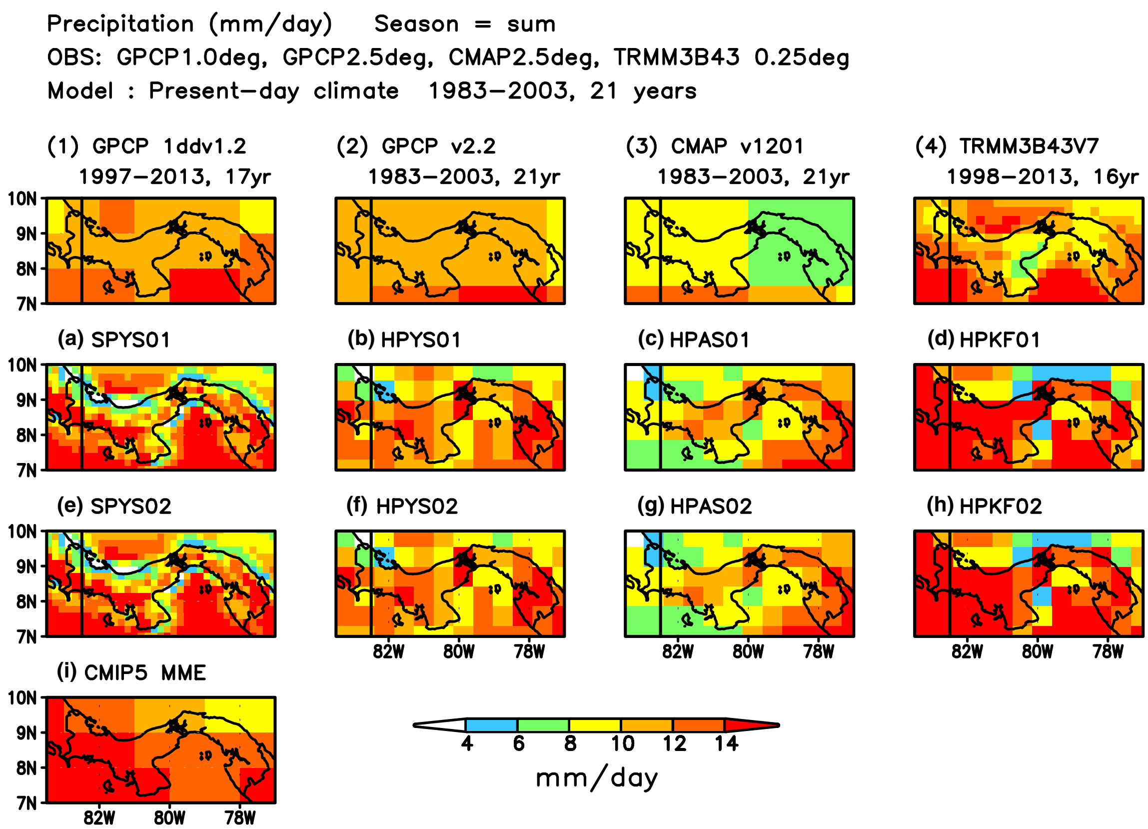

Fig. 2 The climatology of summer (June–August) precipitation over Panama. Unit is mm day^{-1}. **1–4** Observation (Table 2). **a** The simulation of SPYS01 averaged for 1983-2003 (21 years). **b** Same as **a** but for HPYS01. **c** Same as **a** but for HPAS01. **d** Same as **a** but for HPKF01. **e–h** Same as **a–d** but for member 02. **i** CMIP5 MME average (Table S1). Black lines at 82.5°W show the location of latitudinal cross section of Figs. S2 and S3

over sea as well as larger precipitation on the Pacific Ocean side. The present-day simulations using the 20-km model (Fig. 2a, e) reproduce observed distribution well. As for the 60-km model implemented with the YS scheme (Fig. 2b, f), smaller scale precipitation features over land are not well simulated due to coarser horizontal resolution compared to the 20-km model (Fig. 2a, e). In case of the 60-km model implemented with the AS scheme (Fig. 2c, g) and with KF (Fig. 2d, h), smaller scale precipitation features over land are also not well simulated. As for the 60-km model implemented with the AS scheme (Fig. 2c and g), precipitation in the western part of Panama is underestimated compared with observations by Fig. 2(1), (2), (4). For the 60-km model implemented with the KF scheme (Fig. 2d, h), precipitation over land is overestimated. Small scale topographic structure represented by the 20-km model may lead to improve the simulation of summer precipitation over Panama (Figs. S1 and S2).

The simulations of second atmospheric initial conditions (Fig. 2e–h) is almost identical to those of the first atmospheric initial conditions (Fig. 2a–d), indicating the distribution of precipitation is not sensitive to atmospheric initial condition.

The 20-km and 60-km models (Fig. 2a–h) tend to have a band of drier condition over the Caribbean coast of panama, especially SPYS01 (Fig. 2a) and SPYS02 (Fig. 2e) simulations. This may be attributed to forced upward motion by model topography (Fig. S3). In summer (June to August), prevailing low level humid wind is easterly or northeasterly over Panama (Fig. S4). Therefore, orographic precipitation tends to concentrate over mountains as well as lee side of winds. In contrast, this concentration of precipitation leads to the relatively small rainfall over the Caribbean coastal side of Panama.

In case of the MME average (Fig. 2i) of the CMIP5 atmospheric models (Table S1), simulations slightly capture the smaller precipitation on the sea side of the Caribbean Sea, but fails to reproduce small scale structure owing to lower horizontal resolution compared to the 20-km (Fig. 2a, e) and 60-km models (Fig. 2b–d, f–h). If we look into individual CMIP5 models (Fig. S5), many of models over estimate precipitation over whole Panama region and only several models (Figs. S5d, e, n, o, p) show the smaller precipitation on the Caribbean Sea side.

The bias as well as Root Mean Square Error (RMSE) of models were evaluated against the observation of GPCP 1ddv1.2 (Fig. 3a). Colored characters denote the 20-km model (S) and the 60-km model (H). Different colors indicate different cumulus convection schemes. Black characters and marks show the CMIP5 models. Both the 20-km and 60-km models show relatively smaller bias and RMSE than individual CMIP5 models (Table S1). Smaller biases of the 20-km and 60-km models (Fig. S6 as compared with those of CMIP5 models (Fig. S7) are also confirmed by the distributions of individual models.

We plotted observations by the GPCP data with 2.5° grid size (green diamond) and the CMAP data with 2.5° grid size (green square) to show the uncertainty of observation. The spread among observations (green marks) is less than that of models (black and colored characters).

We have also calculated the skill of spatial distribution of precipitation derived from the MME average of CMIP5 models (black circle). We also evaluated the average skill using the individual CMIP5 models (AVM, black square). Firstly, we calculated the skill of spatial pattern of precipitation reproduced by individual models. Then, we averaged all the 24 skill scores to get AVM. If the skill measure is a linear operation such as average and bias, the AVM exactly coincides with the MME average. If skill measure is a nonlinear operation such as RMSE, correlation coefficient and standard deviation, the MME average differs from the AVM. In Fig. 3a, the RMSE of the MME average (black circle) is less than that of most CMIP5 models and the AVM. This is in line with previous studies indicating that the MME average tends to be better than individual model skill in model experiments (Lambert and Boer 2001; Gleckler et al. 2008; Reichler and Kim 2008; Kusunoki and Arakawa 2015; Kusunoki 2017b). The RMSEs and biases of the 20-km and 60-km models (colored characters) are less or equal to that of MME average (black circle) and the AVM (black square).

In addition to RMSE and bias, we introduced the Taylor diagram (Taylor 2001) to graphically illustrate the spatial correlation coefficient between observation and the simulations as well as spatial standard deviation (Fig. 3b). In the Taylor diagram, the radial distance from the origin point is set be proportional to the standard deviation of a simulated spatial pattern normalized with the observed standard deviation. The radial distance of one means perfect simulation as to standard deviation of spatial distribution. The angle from the y-axis specifies the correlation coefficient between the observed and simulated distribution. The location of green circle means the perfect simulation. Similar to Fig. 3a, two other observations as well as the MME average and the AVM are shown. In this diagram, 10 CMIP5 models (a, d, h, i, l, m, n, o, u, v) out of 24 models are plotted out of the quadrant domain, while all the 20-km and 60-km models are plotted in the domain. In terms of Taylor diagram, the performance of the 20-km and 60-km models (colored characters) are higher than or equal to the CMIP5 individual models (black characters), those of the MME average (black circle) and the AVM (black square).

Further, we have calculated the RMSE of precipitation over Panama for all four seasons and annual mean (Fig. S8). The RMSE in summer tends to be larger than other seasons,

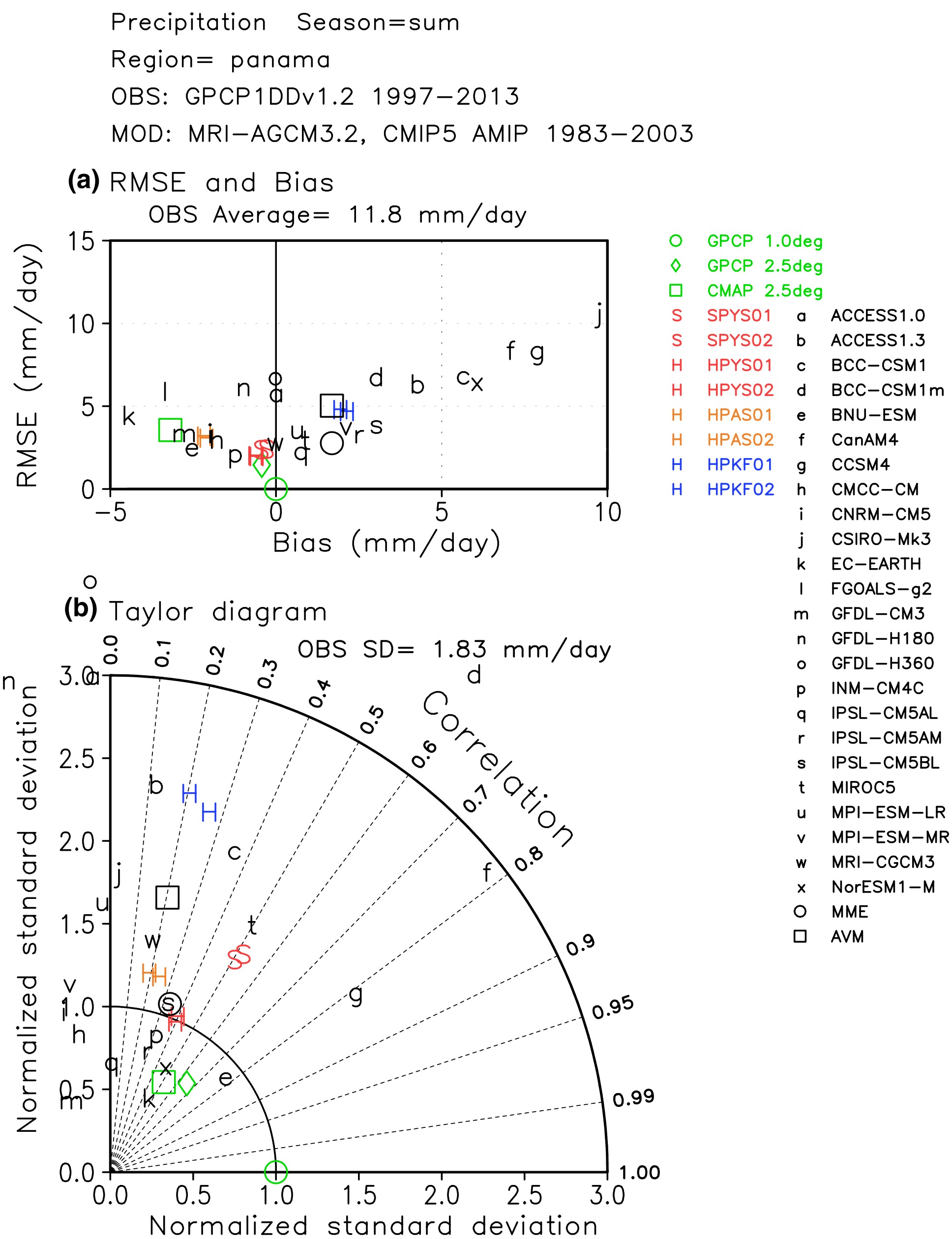

Fig. 3 Skill of summer precipitation simulated by models verified against the GPCP 1dd v1.2 data (green circle) over Panama (83.5°–77°W, 7°–10°N). The target domain is the same as in Fig. 2. Green marks denote other observations (Table 2). Colored characters show the MRI-AGCM3.2 models. S means the 20-km model. H means the 60-km model. Red, orange and blue characters denote the YS, AS and KF cumulus schemes, respectively. Black characters show the CMIP5 individual models (Table S1). Black circles indicate the MME mean. Black squares indicate the average of skill scores of all the CMIP5 models (AVM). **a** The root mean square error (RMSE) and bias. Unit is mm day^{-1}. The domain average of observation is shown above the panel. **b** The Taylor diagram for displaying pattern statistics (Taylor 2001). The radial distance from the origin is proportional to the standard deviation of a simulated pattern normalized by the observed standard deviation. The spatial correlation coefficient between the observed and simulated fields is given by angle from *y* axis. The standard deviation of the observation in the domain is shown above the panel

suggesting the simulation of summer precipitation is most difficult of all four seasons. In general, the RMSEs of the 20-km and 60-km models are less than or equal to the individual CMIP5 models (black line) and the AVM (green line) except for HPKF (blue line) in autumn. The RMSEs of the MME average of CMIP5 model (green circles) is the smallest of all the model except for summer. Some of the 20-km and 60-km models shows comparable performance in terms of MME average (green circles).

Seasonal March of ITCZ over the Central America including Panama (83.5°–77.0°W, 10°S–15°N) is well reproduced with the MRI-AGCM3.2 models (Fig. S9) and CMIP5 models (Fig. S10). The MRI-AGCM3.2 models generally overestimate precipitation for the latitudes for 10°S–15°N, but the 60-km models with the AS scheme (Fig. S9c and S9g) tend to underestimate precipitation in the rainy season over Panama (7°–10°N). The ITCZ simulated by the CMIP5 models simulate excessive rainfall (Fig. S12). In terms of quantitative skill measures, the MRI-AGCM3.2 models are superior or similar to the CMIP5 models as to precipitation over the latitudes for equator to 15°N (Fig. S13) and over Panama from 7° to 10°N (Fig. S14).

In summary, the 20-km and 60-km models perform better than the CMIP5 models as to seasonal and annual mean precipitation, and seasonal March of ITCZ over Panama.

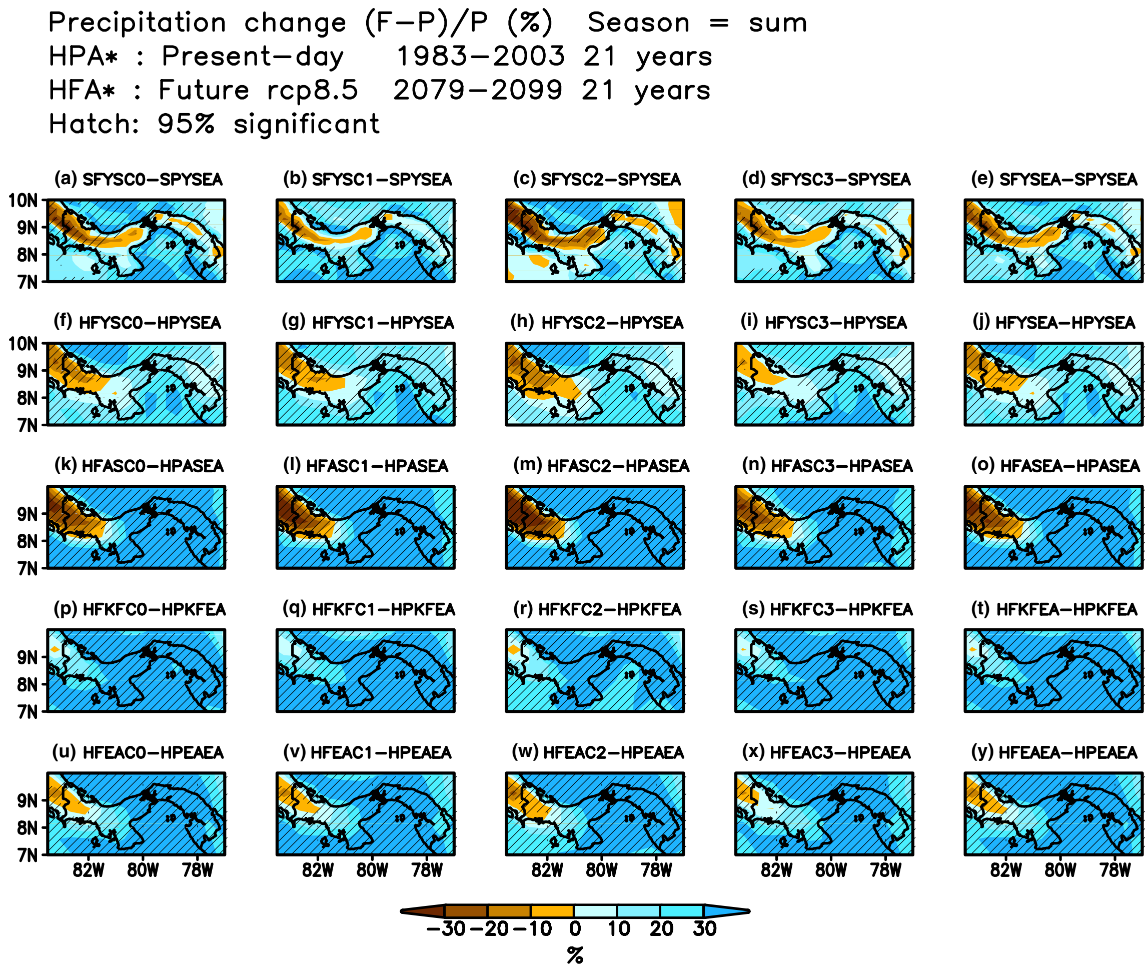

Fig. 4 Future changes (2079–2099) in summer (June–August) precipitation (%) from the present-day climatology (1983–2003). Change is normalized by the present-day climatology. Hatched regions show changes above the 95% significance level based on Student's t test. The ensemble average is used for the present-day climate simulations. 1 st row: **a–e** The 20-km model with the YS scheme. 2nd row: The 60-km model with the YS scheme. 3rd row: The 60-km model with the AS scheme. 4th row: The 60-km model with the KF scheme. 5th row: The ensemble average of 60-km model with the three convection schemes (2nd to 4th rows). 1st column; **a, f, k, p, u** Simulations with the SST cluster C0. 2nd column: Simulations with C1. 3rd column: Simulations with C2. 4th column: Simulations with C3. 5th column: The ensemble average of simulations with the four SSTs (1st to 4th columns)

5 Future climate change

5.1 Changes in summer precipitation

Future precipitation changes in summer (June–August) projected by the 20-km and 60-km models are depicted by Fig. 4. As for SFYSC0 (Fig. 4a), the preset-day climate SPYSEA is obtained by averaging two simulations SPYS01 and SPYS02. Future change is calculated by subtracting the present-day climate SPYSEA from the future simulation SFYSC0. Then, this change is converted into the ratio to the present-day climatology SPYSEA. Similar method is applied for SFYSC1 (Fig. 4b), SFYSC2 (Fig. 4c) and SFYSC3 (Fig. 4d) simulations. As for the 60-km model (Fig. 4f–i, k–n, p–s), future changes are obtained using the present-day and future simulations implemented with the same cumulus convection schemes.

The Student's t test method was applied to calculate statistical significance of changes using variances of year-to-year variability. Since the degree of freedom (DOF) in ensemble simulation is much larger than individual simulations, we can enhance statistical significance of future change derived by ensemble simulations.

As for SFYSC0 (Fig. 4a), precipitation increases over ocean, but decreases over land. This spatial pattern is similarly represented in simulations for other SSTs of C1 (Fig. 4b), C2 (Fig. 4c) and C3 (Fig. 4d). As a result, the ensemble average (Fig. 4e) shows the increase of precipitation over oceans and decrease over land. In the case of 60-km model using the YS scheme (Fig. 4f–l; the 2nd row),

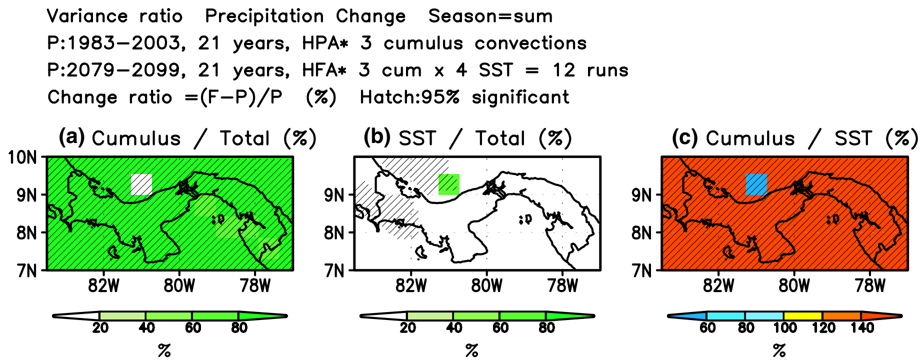

Fig. 5 A two way of ANalysis Of VAriance (ANOVA; Storch and Zwiers 1999) applied to future summer (June–August) precipitation changes by 12 ensemble simulations of the 60-km model with respect to three different cumulus convection schemes and four different SST distributions (Fig. 4f–i, k–n, p–s). **a** Relative contribution of cumulus convection scheme as the ratio to the total variance (%). **b** Relative contribution of SST as the ratio to the total variance (%). **c** Ratio (%) of the variance by cumulus convection scheme (**a**) to the variance by SST (**b**). Hatches show regions above the 95% significance level based on *F* test

the reduction of precipitation is restricted in the western part of Panama. Similar change pattern is also presented for the 60-km model using the AS scheme (Fig. 4k–o; the 3rd row) like the 60-km model using the YS scheme (Fig. 4f–j), but the increase of precipitation over oceans is much larger. As for the 60-km model using the KF scheme (Fig. 4p–t; the 4th row), precipitation increases over the whole domain. In terms of ensemble average (Figs. 4u-x: the bottom row) with respect to the different cumulus convection schemes, spatial distributions of change are almost similar. On the other hand, in terms of ensemble average (Fig. 4e, j, o, t; the last column) with respect to the different SST distributions, spatial distributions of change differs, especially the 60-km model implemented with the KF scheme (Fig. 4t). This suggests that future precipitation changes largely depend upon cumulus convection scheme and not to SST distribution. The increase of precipitation over the eastern part of Panama represented in the ensemble average based on the 60-km model (Fig. 4y) is larger than that that of the 20-km model (Fig. 4e). This is due to the significant precipitation increase over the eastern part of Panama in the simulation by the 60-km model implemented with the AS scheme (Fig. 4k–o; the third row) and KF scheme (Fig. 4p–t; the fourth row).

5.2 What controls precipitation change, cumulus convection scheme or SST?

For the purpose of evaluating the relative contribution of cumulus convection scheme and SST upon precipitation change in the future, we have applied a two way of ANalysis Of VAriance (ANOVA; Storch and Zwiers 1999) to the future precipitation changes projected by the twelve-member ensemble simulations of the 60-km model (Fig. 4f–i, k–n, p–s). The ensemble simulations consist of the combination of three kinds of cumulus convection schemes (YS, AS, KF) and four kinds of SST distributions (C0, C1, C2, C3). The ANOVA is able to quantitatively divide the total variance into the relative contributions of the variances arising from variations in cumulus convection schemes and SST distributions. Test S1 explains the details of method. Figure 5a depicts the contribution of cumulus convection scheme to the total variance of 12 simulations (Fig. 4f–i, k–n, p–s). The ratio exceeds 80% over most part of Panama. In contrast, the contribution of SST is small (Fig. 5b). As a result, it is recognized that the effect of cumulus convection scheme is stronger than that of SST as to change in summer precipitation over Panama projected by the 60-km model (Fig. 5c).

5.3 Precipitation change in each month

Figure 6 illustrates the future precipitation changes as to all months derived from all simulations. If we consider that the number of simulation conducted with the 60-km model (three convection schemes) is three times larger than that with the 20-km (one convection scheme), simple average would put too much emphasis on the 20-km model. This leads to biased and inhomogeneous sampling. Therefore, in this paper we consistently give three times larger weight for the 20-km model than for the 60-km model when we make the ensemble average using the 20-km and 60-km models. We calculated the variance in the same weighting method to evaluate the statistical significance of future change.

As for January (Fig. 6a). precipitation increases over oceans with statistical significance (hatched region), but precipitation decreases over some regions in the western and central part of land without statistical significance. In February (Fig. 6b) and March (Fig. 6c), distribution of change patterns are approximately similar to January case (Fig. 6a) with some differences in the location of area where precipitation decreases. In April (Fig. 6d), precipitation generally

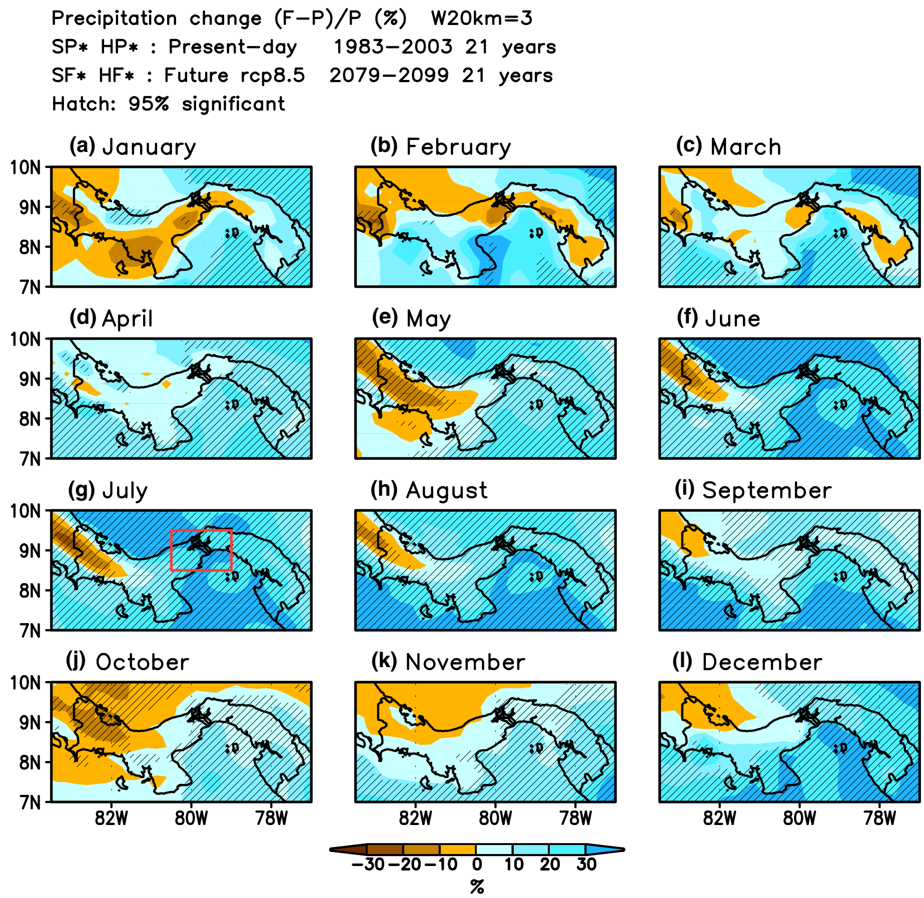

Fig. 6 Future changes in monthly precipitation projected by the all simulations. SFYSEA-SPYSEA and HFEAEA-HPEAEA are averaged, giving three times larger weight for the 20-km model than the 60-km model. Unit is %. Hatched regions show changes above the 95% significance level. In the **g**, the red box indicates the target region (79.0°–80.5°W, 8.5°–9.5°N) for Figs. 8 and S11–13

increases in the whole domain, but the statistical significance is low in the western part of Panama. From May to September (Fig. 6e–i) which corresponds the rainy season of Panama, precipitation increases over oceans and the central and eastern part of Panama, but precipitation decreases over the land of western Panama. Increase of precipitation over oceans from June to September (Fig. 6f–i) is larger than that in January to May (Fig. 6a–e). From October to December (Fig. 6j–l), change patterns are nearly similar to those in January to March (Fig. 6a–c), although the decrease of precipitation over the western part of domain in October is larger than that in any other months. Precipitation consistently increase over oceans and the central and eastern part of Panama from May to September. This suggest the precipitation during the rainy season will increase over these area in the future.

Future precipitation increase in rainy season over Panama is consistent with the previous studies based on CMIP3 models, CMIP5 models and the MRI-AGCM3.2H (Fig. 14.19 in Christensen et al. 2013), although their projections are based on the SSTs of former generation CMIP3 models and former generation emission scenario of A1B.

5.4 Why precipitation changes?

The future precipitation change are tightly connected to the change in the large scale motion of atmosphere. Figure 7a illustrates the vertically integrated water vapor flux (arrow) for July corresponding to the middle of the rainy season of Panama. In the same panel, we also showed the precipitation rate converted from the convergence of flux (color). Increase of precipitation over most regions (Fig. 7b) can be attributed to the increase of water vapor advected from the Caribbean Sea which converges over Panama. Convergence over the western part of Panama is smaller than other regions, which is not consistent with the decreased precipitation change (Fig. 7b). This may be partly due to the low horizontal resolution of water vapor and wind field with 1.25° grid size. We could not archive 3-dimensional wind and moisture field in the original horizontal resolution of 20-km and 60-km because of huge data amount. The 1.25° grid size corresponds to about 138 km spacing which is too coarse to represent high mountains in the western part of Panama. The lack of orography effect in the 3-dimensional wind and moisture field may lead to the discrepancy between precipitation change (Fig. 7b) and moisture convergence (Fig. 7a) over the western part of Panama. Figure 7 is based on ensemble

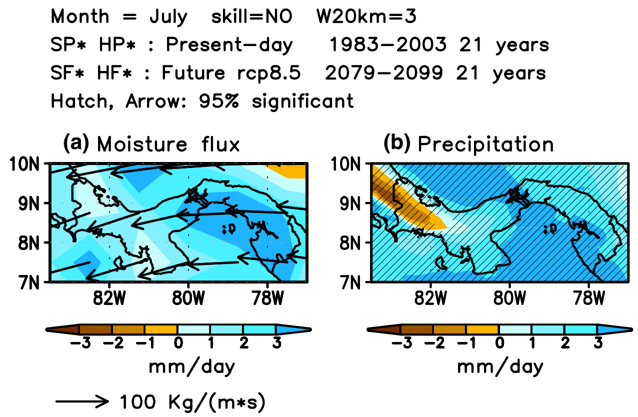

Fig. 7 Comparison between water vapor flux change and precipitation change for July. The ensemble averages of all simulations with three times larger weight for the 20-km model than the 60-km model are illustrated. **a** The vertically integrated water vapor flux (arrow; kg $m^{-1}s^{-1}$) and its convergence (shading; mm day^{-1}). The unit of convergence is converted to mm day^{-1} assuming the density of liquid water as 1 g cm^{-3}. Arrow is plotted only if change is above the 95% significance level. **b** Precipitation. Hatched regions show changes above the 95% significance level. Same as Fig. 6g but for different unit

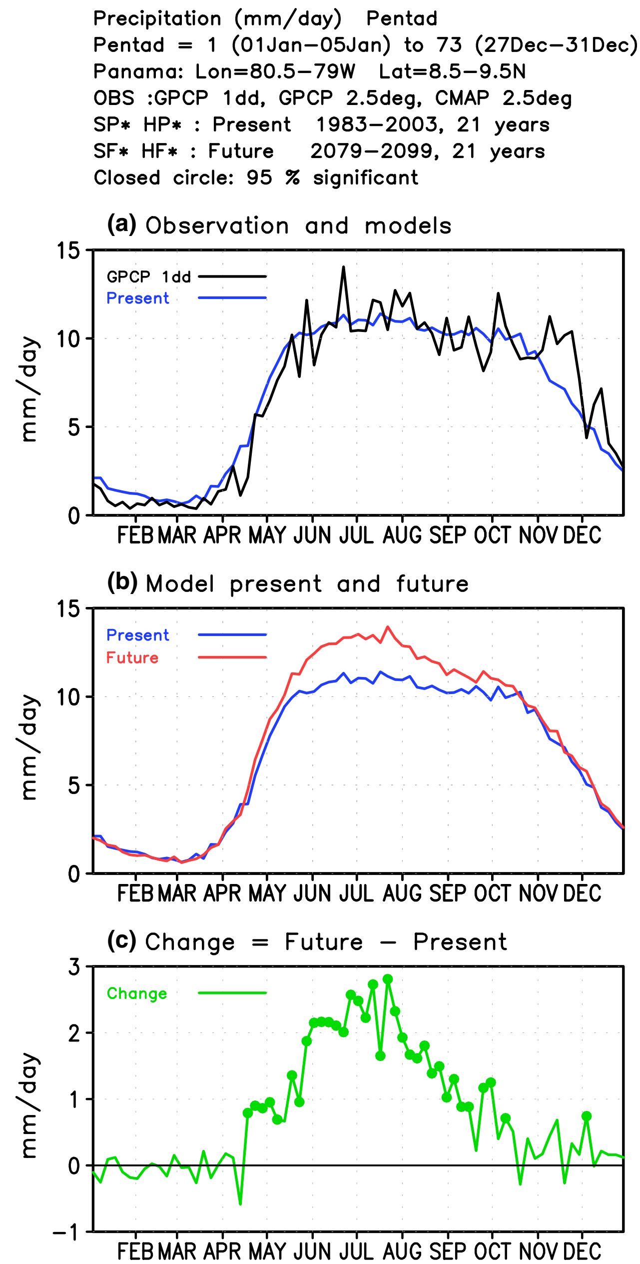

Fig. 8 Time evolutions of pentad mean precipitation averaged over the Panama canal throughout the year. The target region (79.0°–80.5°W, 8.5°–9.5°N) is indicated by the red box in Fig. 6g. Unit is mm day^{-1}. The ensemble averages of all simulations with three times larger weight for the 20-km model than the 60-km model are illustrated. **a** Observations of GPCP 1ddv1.2 (black) and the present-day climatology by the models (blue). **b** The present-day climatology (blue) and the future climatology (red). **c** Future change (green). Closed circles show changes above the 95% significance level

average which might mix up correspondence between flux convergence and precipitation change in each runs.

Rauscher et al. indicated that a future southward displacement of the ITCZ resulting in a wetter panama and drier northern Central America. Our results are partly consistent with their results in that some part of Central America show drier condition (Fig. S15). However, southward shift of ITCZ is not so evident in our case (Figs S15-18). In our experiments, change of precipitation over Panama is largely determined by two mechanisms. One is the precipitation increase over the ITCZ without any large location change of the ITCZs (Fig. S16). This mechanism determines large scale structure of precipitation change over Panama region. The other is the orographic effect. Increased moisture transport from Caribbean sea to Panama (Fig. 7a) enhances orographic precipitation on the lee side of mountains resulting in the decrease of precipitation over mountains in western part of Panama (Fig. S16). This second mechanism determines small scale structure of precipitation change over Panama region.

5.5 Regional average precipitation over the Panama canal

We further investigated the seasonal March of precipitation averaged over the Panama canal, the Gatun lake and related river basin (79.0°–80.5°W, 8.5°–9.5°N). The red box in Fig. 6g defines the target region. Figure 8a illustrates the observed and simulated pentad precipitation in the present-day climate. The model simulation is the total ensemble averages using the 20-km and 60-km models. The model simulates very well not only the amount of precipitation but also the date of onset and retreat of rainy season. Individual simulations (Fig. S19) also simulate well the time evolution of precipitation except for the 60-km models implemented

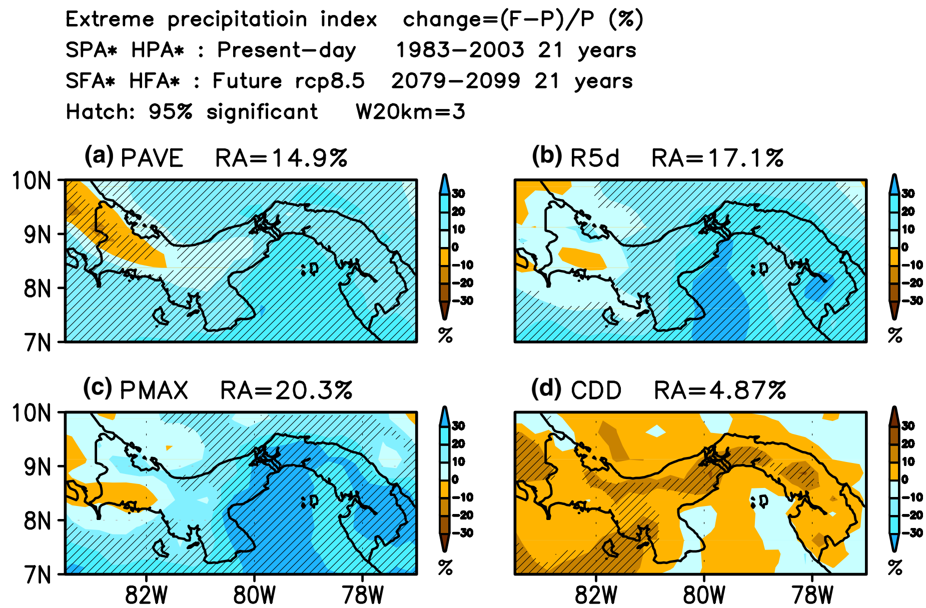

Fig. 9 Future changes in extreme precipitation events (annual statistics, Table 3) projected by the all simulations. Unit is %. Hatched regions show changes above the 95% significance level. **a** Annual precipitation (PAVE). **b** Maximum 5-day precipitation total (R5d). **c** Maximum 1-day precipitation (PMAX). **d** Consecutive dry days (CDD). Note that color bar is reversed for CDD. Values of RA in the captions of each panels denote domain average

with the KF scheme (HPKF, green lines). Figure 8b compares the present-day climate simulations and future climate simulations. Future precipitation will increases during the rainy season from May to October. In contrast, the date of onset and retreat of rainy season is almost same. On the other hand, precipitation in dry season from December to April does not change in the future. See Fig. S20 for individual simulations. Future increase of precipitation in the rainy season is statistically significant (Fig. 8c). Individual simulations (Fig. S21) also show similar change, although the 60-km models with the KF scheme (HFKF, green lines) only project decrease of precipitation in May. These result suggest that the planning of water resource management for the Panama canal may require some modification in the future.

The CMIP3 models, CMIP5 models, MRI-AGCM3.1 (Fábrega et al. 2013) and the MRI-AGCM3.2H project larger precipitation increase in rainy season than in dry season (Christensen et al. 2013). Our results are partly consistent with their findings, although their projections are based on the SSTs of former generation CMIP3 models and former generation emission scenario of A1B.

5.6 Extreme precipitation events

Three indices were selected from ten measures of climate extreme events defined in Frich et al. (2002). The simple daily precipitation intensity index (SDII) is usually adopted to verify climate models. The maximum 5-day precipitation total (R5d) also define another precipitation intensity. Furthermore, we adopted the maximum 1-day precipitation total (PMAX) to measure most intense precipitation. In contrast, consecutive dry days (CDD) is an index measuring dryness of atmosphere and drought. For comparison, annual precipitation (PAVE) is also calculated. Table 3 summarizes four indices introduced here. These indices are based on annual statistics. R5d and PMAX are regarded as appropriate indicator to evaluate the potential of natural disaster such as flood, inundation and land slide.

Figure 9a shows future changes of PAVE projected by all simulations using the 20-km and 60-km models. PAVE increases over almost all area except for the land in the western part of Panama. The spatial pattern of change in R5d (Fig. 9b) is nearly same as that in PAVE (Fig. 9a), but the increase of R5d over the Pacific Ocean is larger than that of PAVE. The spatial pattern of change in PMAX (Fig. 9c) is almost similar to that in R5d (Fig. 9b), but the increase of precipitation of PMAX is larger than that of R5d. In terms of regional average (RA), the increase of precipitation is the largest for PMAX (Fig. 9c) but the smallest for PAVE (Fig. 9a), indicating the increase of severe precipitation event is much more distinct than that of weak and moderate precipitation. These changes agree with the previous investigation over the CAC (Nakaegawa et al. 2014c) where the MRI-AGCM3.1 is forced with SRES A1B SST. Also, this tendency is consistent with previous studies by Kusunoki and Mizuta (2013) and Kusunoki (2017a, b), although their target region is East Asia and global domain.

On the other hand, CDD increases over most regions over Panama (Fig. 9d), suggesting the increase of possibility of drought. The increase of intense precipitation as well as drought means the modification of water resource management in the future, especially over the Panama canal and related river basin regions.

6 Conclusions

Our results are summarized as follows:

1. The performance of MRI-AGCM3.2 models is higher than or similar to CMIP5 atmospheric models with respect to the geographical distribution and seasonal March of precipitation over Panama.
2. In the future, precipitation will increase over the central and eastern part of Panama from May to November corresponding to the rainy season of Panama.
3. Uncertainty of future precipitation change depends on cumulus convection schemes rather than SST distributions.
4. Increase of precipitation over most regions can be attributed to the increase of water vapor transport originating in the Caribbean Sea which converges over Panama.
5. Precipitation averaged over the Panama canal, the Gatun lake and related river basin will increase during the rainy season from May through October, while precipitation in dry season from December through April does not change in the future.
6. Due to annual statistics, intense precipitation increases, whereas the possibility of drought increases over Panama.
7. These future change in precipitation suggest that the planning of water resource management for the Panama canal may require some modification in the future.

Acknowledgements This work was supported by the research project " Integrated Research Program for Advanced Climate Modeling" under the framework of the TOUGOU Program of the Ministry of Education, Culture, Sports, Science, and Technology (MEXT) of Japan. We appreciate advice and comments by anonymous reviewers which enhanced the quality of manuscript. We also thanks the colleagues of global climate modelling in MRI. The National System of Investigation (SNI) of Secretaría Nacional de Ciencia, Tecnología e Innovación (SENACYT) supports the research activities by J. E. Sanchez-Galan, R. Pinzón, and J. R. Fábrega.

References

Adler RF, Huffman GJ, Chang A, Ferrano R, Xie PP, Janowiak J, Rudolf B, Schneider U, Curtis S, Bolvin D, Gruber A, Susskind J, Arkin P, Nelkin E (2003) The Version-2 Global Precipitation Climatology Preject (GPCP) monthly precipitation analysis (1979–present). J Hydrometeor 4:1147–1167. https://doi.org/10.1175/1525-7541(2003)004%3c1147:TVGPCP%3e2.0.CO;2

Alfaro EJ (2002) Some characteristics of the annual precipitation cycle in Central America and their relationships with its surrounding tropical oceans. Top Meteoro Oceanog 9:88–103. http://hdl.handle.net/10669/15428

Amador JA (1998) A climatic feature of the tropical Americas: the trade wind easterly jet. Top Meteor Oceanogr 5:91–102

Amador JA (2008) The Intra-Americas Seas low-level jet (IALLJ): overview and future research. Ann N Y Acad Sci 1146:153–188. https://doi.org/10.1196/annals.1446.012

Amador JA, Alfaro EJ, Lizano OG, Magana VO (2006) Atmospheric forcing of the eastern tropical Pacific: a review. Prog Oceanogr 69:101–142. https://doi.org/10.1016/j.pocean.2006.03.007

Amador JA, Duran-Quesada AM, Rivera ER, Mora G, Saenz F, Calderon B, Mora N (2016a) The easternmost tropical Pacific. Part II: seasonal and intraseasonal modes of atmospheric variability. Rev Biol Trop 64:S23–S57. https://doi.org/10.15517/rbt.v64i1.23409

Amador JA, Rivera ER, Duran-Quesada AM, Mora G, Saenz F, Calderon B, Mora N (2016b) The easternmost tropical Pacific. Part I: a climate review. Rev de Biol Trop 64:S1–S22. https://doi.org/10.15517/rbt.v64i1.23407

Bengtsson L, Hodges KI, Keenlyside N (2009) Will extratropical storms intensify in a warmer climate? J Clim 22:2276–2301. https://doi.org/10.1175/2008JCLI2678.1

Christensen JH, Krishna Kumar K, Aldrian E, An S-I, Cavalcanti IFA, de Castro M, Dong W, Goswami P, Hall A, Kanyanga JK, Kitoh A, Kossin J, Lau N-C, Renwick J, Stephenson DB, Xie S-P, Zhou T (2013) Chapter 14; Climate Phenomena and their Relevance for Future Regional Climate Change. In: Stocker TF, Qin D, Plattner G-K, Tignor M, Allen SK, Boschung J, Nauels A, Xia Y, Bex V, Midgley PM (eds) Climate change 2013: the physical science basis. Contribution of working group I to the fifth assessment report of the intergovernmental panel on climate change. Cambridge University Press, Cambridge, New York

Collins M, Knutti R, Arblaster J, Dufresne J-L, Fichefet T, Friedlingstein P, Gao X, Gutowski WJ, Johns T, Krinner G, Shongwe M, Tebaldi C, Weaver AJ, Wehner M (2013) Chapter 12; Long-term Climate Change: Projections, Commitments and Irreversibility. In: Stocker TF, Qin D, Plattner G-K, Tignor M, Allen SK, Boschung J, Nauels A, Xia Y, Bex V, Midgley PM (eds) Climate change 2013: The physical science basis. Contribution of working group I to the fifth assessment report of the intergovernmental panel on climate change. Cambridge University Press, Cambridge, New York

Cook KH, Vizy EK (2010) Hydrodynamics of the Caribbean Low-Level Jet and its relationship to precipitation. J Clim 23:1477–1494. https://doi.org/10.1175/2009JCLI3210.1

Endo H, Kitoh A, Ose T, Mizuta R, Kusunoki S (2012) Future changes and uncertainties in Asian precipitation simulated by multiphysics and multi-sea surface temperature ensemble experiments with high-resolution Meteorological Research Institute atmospheric general circulation models (MRI-AGCMs). J Geophys Res 117:D16118. https://doi.org/10.1029/2012JD017874

Enfield DB, Alfaro EJ (1999) The dependence of Caribbean rainfall on the interaction of the tropical Atlantic and Pacific Oceans. J Clim 12:2093–2103. https://doi.org/10.1175/1520-0442(1999)012%3c2093:TDOCRO%3e2.0.CO;2

Fábrega J, Nakaegawa T, Pinzón R, Nakayama K, Arakawa O, SOUSEI Theme-C modeling group (2013) Hydroclimate projections for Panama in the 21st Century. Hydrol Res Lett 7:23–29. https://doi.org/10.3178/hrl.7.23

Flato G, Marotzke J, Abiodun B, Braconnot P, Chou SC, Collins W, Cox P, Driouech F, Emori S, Eyring V, Forest C, Gleckler P, Guilyardi E, Jakob C, Kattsov V, Reason C, Rummukainen M (2013) Chapter 9; Evaluation of Climate Models. In: Stocker TF, Qin D, Plattner G-K, Tignor M, Allen SK, Boschung J, Nauels A, Xia Y, Bex V, Midgley PM (eds) Climate change 2013: the physical science basis. Contribution of working group I to the fifth assessment report of the intergovernmental panel on climate change. Cambridge University Press, Cambridge, New York

Frich P, Alexander LV, Della-Marta P, Gleason B, Haylock M, Klein Tank AMG, Peterson T (2002) Observed coherent changes in climatic extremes during the second half of the twentieth century. Clim Res 19:193–212. https://doi.org/10.3354/cr019193

Gamble DW, Curtis S (2008) Caribbean precipitation: review, model and prospect. Prog Phys Geogr 32:265–276. https://doi.org/10.1177/0309133308096027

Giannini A, Kushnir Y, Cane MA (2000) Interannual variability of Caribbean rainfall, ENSO, and the Atlantic Ocean. J Clim 13:297–311. https://doi.org/10.1175/1520-0442(2000)013%3c0297:IVOCRE%3e2.0.CO;2

Gleckler PJ, Taylor KE, Doutriaux C (2008) Performance metrics for climate models. J Geophys Res 113:D06104. https://doi.org/10.1029/2007JD008972

Graham NE, Georgakakos KP, Vargas C, Echevers M (2006) Simulating the value of El Niño forecasts for the Panama Canal. Adv Water Resour 29:1665–1677. https://doi.org/10.1016/j.advwatres.2005.12.005

Hastenrath S (1978) On modes of tropical circulation and climate anomalies. J Atmos Sci 35:2222–2231. https://doi.org/10.1175/1520-0469(1978)035%3c2222:OMOTCA%3e2.0.CO;2

Hidalgo HG, Alfaro EJ (2015) Skill of CMIP5 climate models in reproducing 20th century basic climate features in Central America. Int J Climatol 35:3397–3421. https://doi.org/10.1002/joc.4216

Hidalgo HG, Amador JA, Alfaro EJ, Quesada B (2013) Hydrological climate change projections for Central America. J Hydrol 495:94–112. https://doi.org/10.1016/j.jhydrol.2013.05.004

Hidalgo HG, Alfaro EJ, Quesada-Montano B (2017) Observed (1970–1999) climate variability in Central America using a high-resolution meteorological dataset with implication to climate change studies. Clim Change 141:13–28. https://doi.org/10.1007/s10584-016-1786-y

Huffman GJ, Adler RF, Morrissey MM, Bolvin DT, Curtis S, Joyce R, McGavock B, Susskind J (2001) Global precipitation at one-degree daily resolution from multisatellite observations. J Hydrometeor 2:36–50. https://doi.org/10.1175/1525-7541(2001)002%3c0036:GPAODD%3e2.0.CO;2

Huffman GJ, Adler RF, Bolvin DT, Gu G, Nelkin EJ, Bowman KP, Hong Y, Stocker EF, Wolff DB (2007) The TRMM multisatellite precipitation analysis (TMPA): quasi-global, multiyear, combined-sensor precipitation estimates at fine scales. J Hydrometeor 8:38–55. https://doi.org/10.1175/JHM560.1

Imbach P, Molina L, Locatelli B, Roupsard O, Mahé G, Neilson R, Corrales L, Scholze M, Ciais P (2012) Modeling potential equilibrium states of vegetation and terrestrial water cycle of Mesoamerica under climate change scenarios. J Hydrometeor 13:665–680. https://doi.org/10.1175/JHM-D-11-023.1

Imbach P, Chou SC, Lyra A, Rodrigues D, Rodriguez D, Latinovic D, Siqueira G, Silva A, Garofolo L, Georgiou S (2018) Future climate change scenarios in Central America at high spatial resolution. PLoS One 13(4):e0193570. https://doi.org/10.1371/journal.pone.0193570

IPCC (Intergovermental Panel on Climate Change) (2013) Climate change 2013: the physical science basis. Contribution of working group I to the fifth assessment report of the intergovernmental panel on climate change. In: Stocker TF, Qin D, Plattner GK, Tignor M, Allen SK, Boschung J, Nauels A, Xia Y, Bex V, Midgley PM (eds). Cambridge University Press, Cambridge, New York

IPCC (2000) Special report on emissions scenarios. A special report of working group III of the intergovernmental panel on climate change. In: Nakicenovic N, Alcamo J, Davis G, deVries B, Fenhann J, Gaffin S, Gregory K, Grübler A, Yong Jung T, Kram T, La Rovere EL, Michaelis L, Mori S, Morita T, Pepper W, Pitcher H, Price L, Riahi K, Roehrl A, Rogner HH, Sankovski A, Schlesinger M, Shukla P, Smith S, Swart R, van Rooijen S, Victor N, and Dadi Z (eds). Cambridge University Press, Cambridge

Kain JS, Fritsch JM (1990) A one-dimensional entraining/detraining plume model and its application in convective parameterization. J Atmos Sci 47:2784–2802. https://doi.org/10.1175/1520-0469(1990)047%3c2784:AODEPM%3e2.0.CO;2

Kusunoki S (2016) Is the global atmospheric model MRI-AGCM3.2 better than the CMIP5 atmospheric models in simulating precipitation over East Asia? Clim Dyn. https://doi.org/10.1007/s00382-016-3335-9

Kusunoki S (2017a) Future changes in precipitation over East Asia projected by the global atmospheric model MRI-AGCM3.2. Clim Dyn. https://doi.org/10.1007/s00382-016-3499-3

Kusunoki S (2017b) Future changes in global precipitation projected by the atmospheric model MRI-AGCM3.2H with a 60-km size. Atmosphere 8:93. https://doi.org/10.3390/atmos8050093

Kusunoki S, Arakawa O (2015) Are CMIP5 models better than CMIP3 models in simulating precipitation over East Asia? J Clim 28:5601–5621. https://doi.org/10.1175/JCLI-D-14-00585.1

Kusunoki S, Mizuta R (2013) Changes in precipitation intensity over East Asia during the 20th and 21st centuries simulated by a global atmospheric model with a 60 km grid size. J Geophys Res Atmos 118:11007–11016. https://doi.org/10.1002/jgrd.50877

Lambert SJ, Boer GJ (2001) CMIP1 evaluation and intercomparison of coupled climate models. Clim Dyn 17:83–106. https://doi.org/10.1007/PL00013736

Magaña V, Amador JA, Medina S (1999) The midsummer drought over Mexico and Central America. J Clim 12:1577–1588. https://doi.org/10.1175/1520-0442(1999)012%3c1577:TMDOMA%3e2.0.CO;2

Maldonado T, Alfaro EJ, Hidalgo HG (2018) A review of the main drivers and variability of Central America's climate and seasonal forecast systems. Rev de Biol Trop 66(Suppl. 1):S153–S175. https://doi.org/10.15517/rbt.v66i1.33294

Mitchell TP, Wallace JM (1992) The annual cycle in equatorial convection and sea surface temperature. J Clim 5:1140–1156. https://doi.org/10.1175/1520-0442(1992)005%3c1140:TACIEC%3e2.0.CO;2

Mizuta R, Adachi Y, Yukimoto S, Kusunoki S (2008) Estimation of the future distribution of sea surface temperature and sea ice using the CMIP3 multi-model ensemble mean. Technical Reports of the Meteorological Research Institute, vol 56, p 28. http://www.mri-jma.go.jp/Publish/Technical/DATA/VOL_56/56_en.html

Mizuta R, Arakawa O, Ose T, Kusunoki S, Endo H, Kitoh A (2014) Classification of CMIP5 future climate responses by the tropical sea surface temperature changes. SOLA 10:167–171. https://doi.org/10.2151/sola.2014-035

Murphy MJ, Georgakakos KP, Shamir E (2014) Climatological analysis of December rainfall in the Panama Canal watershed. Int J Climatol 34:403–415. https://doi.org/10.1002/joc.3694

Nakaegawa T, Kitoh A, Ishizaki Y, Kusunoki S, Murakami H (2014a) Caribbean low-level jets and accompanying moisture fluxes in a global warming climate projected with CMIP3 multi-model ensemble and fine-mesh atmospheric general circulation models. Int J Climatol 34:964–977. https://doi.org/10.1002/joc.3733

Nakaegawa T, Kitoh A, Kusunoki S, Murakami H, Arakawa O (2014b) Hydroclimate change over Central America and the Caribbean in a global warming climate projected with 20-km and 60-km mesh MRI atmospheric general circulation models. Pap Meteorol Geophys 65:15–33. https://doi.org/10.2467/mripapers.65.15

Nakaegawa T, Kitoh A, Murakami H, Kusunoki S (2014c) Maximum 5-day rainfall total and the maximum number of consecutive dry days over Central America in the future climate projected by an atmospheric general circulation model with three different horizontal resolutions. Theor Appl Climatol 116:155–168. https://doi.org/10.1007/s00704-013-0934-9

Nakaegawa T, Arakawa O, Kamiguchi K (2015) Investigation of climatological onset and withdrawal of the rainy season in Panama

Based on a daily gridded precipitation dataset with a high horizontal resolution. J Clim 28:2745–2763. https://doi.org/10.1175/JCLI-D-14-00243.1

Neelin JD, Munnich M, Su H, Meyerson JE, Holloway CE (2006) Tropical drying trends in global warming models and observations. Proc Natl Acad Sci 103:6110–6115. https://doi.org/10.1073/pnas.0601798103

Okada Y, Takemi Ishikawa H, Kusunoki S, Mizuta R (2017) Future changes in atmospheric conditions for the seasonal evolution of the Baiu as revealed from projected AGCM experiments. J Meteor Soc Jpn 95:239–260. https://doi.org/10.2151/jmsj.2017-013

Pinzón R, Hibino K, Takayabu I, Nakaegawa T (2017) Virtual experiencing future climate changes in Central America with MRI-AGCM: climate analogues study. Hydrol. Res Lett 11:106–113. https://doi.org/10.3178/hrl.11.107

Randall DA, Pan DM (1993) Implementation of the Arakawa-Schubert cumulus parameterization with a prognostic closure. In: The representation of cumulus convection in numerical models, meteorological monographs, vol 24, no 46, Chapter 11, pp 137–147

Rauscher SA, Giorgi F, Diffenbaugh NS, Seth A (2008) Extension and Intensification of the Meso-American mid-summer drought in the twenty-first century. Clim Dyn 31:551–571. https://doi.org/10.1007/s00382-007-0359-1

Rayner NA, Parker DE, Horton EB, Folland CK, Alexander LV, Rowell DP, Kent EC, Kaplan A (2003) Global analyses of sea surface temperature, sea ice, and night marine air temperature since the late nineteenth century. J Geophys Res 108(D14):4407. https://doi.org/10.1029/2002JD002670

Reichler T, Kim J (2008) How well do coupled models simulate today's climate? Bull Am Meteor Soc 89:303–311. https://doi.org/10.1175/BAMS-89-3-303

Ropelewski CF, Halpert MS (1987) Global and regional scale precipitation patterns associated with the El Nino/Southern Oscillation. Mon Weather Rev 115:1606–1626. https://doi.org/10.1175/1520-0493(1987)115%3c1606:GARSPP%3e2.0.CO;2

Shibata K, Deushi M, Sekiyama TT, Yoshimura H (2004) Development of an MRI chemical transport model for the study of stratospheric chemistry. Pap Meteor Geophys 55:75–119. https://doi.org/10.2467/mripapers.55.75

Sperber KR, Annamalai H, Kang IS, Kitoh A, Moise A, Turner AG, Wang B, Zhou T (2013) The Asian summer monsoon: an intercomparison of CMIP5 vs. CMIP3 simulations of the late 20th century. Clim Dyn 41:2711–2744. https://doi.org/10.1007/S00382-012-1607-6

Storch HV, Zwiers FW (1999) Section 9 Analysis of variance. In: Storch HV, Zwiers FW (eds) Statistical analysis in climate research. Cambridge University Press, Cambridge, pp 171–192

Taylor KE (2001) Summarizing multiple aspects of model performance in a single diagram. J Geophys Res 106:7183–7192. https://doi.org/10.1029/2000JD90071

Taylor MA, Alfaro E (2005) Climate of Central America and the Caribbean. The encyclopedia of world climatology. J Oliver Ed Spring Press. https://doi.org/10.1007/1-4020-3266-8

Taylor MA, Stephenson TS, Owino A, Chen AA, Campbell JD (2011) Tropical gradient influences on Caribbean rainfall. J Geophys Res 116:D00Q08. https://doi.org/10.1029/2010JD015580

Tiedtke M (1989) A comprehensive mass flux scheme for cumulus parameterization in large-scale models. Mon Weather Rev 117:1779–1800. https://doi.org/10.1175/1520-0493(1989)117%3c1779:ACMFSF%3e2.0.CO;2

Wang C, Enfield DB (2001) The tropical Western Hemisphere warm pool. Geophys Res Lett 28:1635–1638. https://doi.org/10.1029/2000GL011763

Wang C, Lee SK, Enfield DB (2007) Impact of the Atlantic warm pool on the summer climate of the Western Hemisphere. J Clim 20:5021–5040. https://doi.org/10.1175/LCLI4304.1

Wang C, Lee SK, Enfield DB (2008) Climate response to anomalously large and small Atlantic warm pools during the summer. J Clim 21:2437–2450. https://doi.org/10.1175/2007JCLI2029.1

Xie P, Arkin P (1997) Global precipitation: a 17-year monthly analysis based on gauge observations, satellite estimates and numerical model outputs. Bull Am Meteor Soc 78:2539–2558. https://doi.org/10.1175/1520-0477(1997)078%3c2539:GPAYMA%3e2.0.CO;2

Yoshimura H, Mizuta R, Murakami H (2015) A spectral cumulus parameterization scheme interpolating between two convective updrafts with semi-lagrangian calculation of transport by compensatory subsidence. Mon Weather Rev 143:597–621. https://doi.org/10.1175/MWR-D-14-00068.1

Yukimoto S, Yoshimura H, Hosaka M, Sakami T, Tsujino H, Hirabara M, Tanaka T, Deushi M, Obata A, Nakano H, Adachi Y, Shindo E, Yabu S, Ose T, Kitoh A (2011) Meteorological Research Institute–Earth System Model version 1 (MRI-ESM1)—MODEL description. Technical reports of the Meteorological Research Institute, vol 64, p 88. http://www.mri-jma.go.jp/Publish/Technical/DATA/VOL_64/index_en.html